



1 **Role of OH variability in the stalling of the global atmospheric CH<sub>4</sub> growth**  
2 **rate from 1999 to 2006**

3 **J. McNorton<sup>1,2</sup>, M. P. Chipperfield<sup>1,2</sup>, M. Gloor<sup>3</sup>, C. Wilson<sup>1,2</sup>, W. Feng<sup>1,4</sup>,**  
4 **G. D. Hayman<sup>5</sup>, M. Rigby<sup>6</sup>, P. B. Krummel<sup>7</sup>, S. O'Doherty<sup>6</sup>, R. G. Prinn<sup>8</sup>, R. F. Weiss<sup>9</sup>,**  
5 **D. Young<sup>6</sup>, E. Dlugokencky<sup>10</sup>, and S. A. Montzka<sup>10</sup>**

- 6 1. School of Earth and Environment, University of Leeds, Leeds, LS2 9JT, UK.  
7 2. National Centre for Earth Observation, University of Leeds, LS2 9JT, UK.  
8 3. School of Geography, University of Leeds, Leeds, LS2 9JT, UK.  
9 4. National Centre for Atmospheric Science, University of Leeds, LS2 9JT, UK.  
10 5. Centre for Ecology and Hydrology, Wallingford, UK.  
11 6. School of Chemistry, University of Bristol, Bristol, BS8 1TS, UK.  
12 7. CSIRO Oceans and Atmosphere Flagship, Aspendale, Victoria, Australia.  
13 8. Center for Global Change Science, Massachusetts Institute of Technology, Cambridge,  
14 MA 02139, USA.  
15 9. Scripps Institution of Oceanography, University of California, San Diego, CA 92093, USA.  
16 10. National Oceanic and Atmospheric Administration, Boulder, USA.

17 **Abstract**

18 The growth in atmospheric methane (CH<sub>4</sub>) concentrations over the past two decades has shown  
19 large variability on a timescale of many years. Prior to 1999 the globally averaged CH<sub>4</sub>  
20 concentration was increasing at a rate of 6.0 ppb/yr, but during a stagnation period from 1999  
21 to 2006 this growth rate slowed to 0.6 ppb/yr. Since 2007 the growth rate has again increased  
22 to 4.9 ppb/yr. These changes in growth rate are usually ascribed to variations in CH<sub>4</sub> emissions.  
23 We have used a 3-D global chemical transport model, driven by meteorological reanalyses and  
24 variations in global mean hydroxyl (OH) concentrations derived from CH<sub>3</sub>CCl<sub>3</sub> observations  
25 from two independent networks, to investigate these CH<sub>4</sub> growth variations. The model shows  
26 that between 1999 and 2006, changes in the CH<sub>4</sub> atmospheric loss contributed significantly to  
27 the suppression in global CH<sub>4</sub> concentrations relative to the pre-1999 trend. The largest factor  
28 in this is relatively small variations in global mean OH on a timescale of a few years, with  
29 minor contributions of atmospheric transport of CH<sub>4</sub> to its sink region and atmospheric  
30 temperature. Although changes in emissions may be important during the stagnation period,  
31 these results imply a smaller variation is required to explain the observed CH<sub>4</sub> trends. The  
32 contribution of OH variations to the renewed CH<sub>4</sub> growth after 2007 cannot be determined with  
33 data currently available.



## 34 1. Introduction

35 The global mean atmospheric methane ( $\text{CH}_4$ ) concentration has increased by a factor of 2.5  
36 since the pre-industrial era, from approximately 722 ppb in 1750 to  $1803.2 \pm 0.7$  ppb in 2011  
37 (Etheridge et al., 1998; Dlugokencky et al., 2005). Over this time period methane has accounted  
38 for approximately 20% of the total direct anthropogenic perturbation of radiative forcing by  
39 long-lived greenhouse gases ( $0.48 \pm 0.05 \text{ W/m}^2$ ), the second largest contribution after  $\text{CO}_2$   
40 (Cicerone et al., 1988; Myhre et al., 2013). This long-term methane increase has been attributed  
41 to a rise in anthropogenic emissions from fossil fuel exploitation, agriculture, waste  
42 management and biomass burning (Dlugokencky et al., 2011). Predictions of future  $\text{CH}_4$  levels  
43 require a complete understanding of processes governing emissions and atmospheric removal.

44 Since the mid-1980s measurements of  $\text{CH}_4$  in discrete atmospheric air samples collected at  
45 surface sites have been used to observe changes in the interannual growth rate of  $\text{CH}_4$  (Rigby  
46 et al., 2008; Dlugokencky et al., 2011, Kirschke et al., 2013). Nisbet et al. (2014) showed that  
47 between 1984 and 1992 atmospheric  $\text{CH}_4$  increased at  $\sim 12$  ppb/yr, after which the growth rate  
48 slowed to  $\sim 3$  ppb/yr. In 1999 a period of near-zero growth began which continued until 2007.  
49 In 2007 this stagnation period ended and since then average growth has increased again to  $\sim 6$   
50 ppb/yr (Rigby et al., 2008; Dlugokencky et al., 2011).

51 The reasons for the pause in  $\text{CH}_4$  growth are not well understood. Bousquet et al. (2006)  
52 performed an atmospheric transport inversion study to infer an increase in anthropogenic  
53 emissions since 1999. Similarly, the EDGAR v3.2, bottom-up anthropogenic emission  
54 inventory, an updated inventory to that used as an a priori by Bousquet et al. (2006), shows a  
55 year-on-year increase in anthropogenic  $\text{CH}_4$  emissions between 1999 and 2006 (Olivier et al.,  
56 2005). This would suggest that a decrease in anthropogenic emissions is not the likely cause of  
57 the pause in growth during this period. A second explanation is a reduction in wetland  
58 emissions between 1999 and 2006, which is in part compensated by an increase in  
59 anthropogenic emissions (Bousquet et al., 2006). However, more recently, Pison et al. (2013)  
60 used two atmospheric inversions and found much more uncertainty in the role wetlands played  
61 in the pause in growth over this period.

62 Dlugokencky et al. (2003) argued that the behaviour of global mean  $\text{CH}_4$  up to around 2002  
63 was characteristic of the system approaching steady state, accelerated by decreasing emissions  
64 at high northern latitudes in the early 1990s and fairly constant emissions elsewhere. However,  
65 since then there have been notable perturbations to the balance of sources and sinks (Rigby et  
66 al., 2008). This has been, at least partly, attributed to increases in wetland (Bousquet et al.,  
67 2011) and anthropogenic emissions (Bousquet et al., 2006). Recent changes in emissions are  
68 not well constrained and the reasons for the renewed growth are also not fully understood.

69 Atmospheric chemistry has also been hypothesised to play a role in past variations in  $\text{CH}_4$   
70 growth rates. The major (90%) sink of atmospheric  $\text{CH}_4$  is via reaction with the hydroxyl  
71 radical, OH. Variations in the concentration of OH ( $[\text{OH}]$ ), or changes to the reaction rate  
72 through changes in temperature, therefore have the potential to affect  $\text{CH}_4$  growth. Previous  
73 studies have suggested that an increase in atmospheric OH concentration may have been at  
74 least partly responsible for a decrease in the  $\text{CH}_4$  growth rate (Lelieveld et al., 2004; Fiore et



75 al., 2006). This rise in OH has been attributed to an increase in lightning NO<sub>x</sub> (Fiore et al.,  
76 2006). The abundance of other species such as H<sub>2</sub>O, O<sub>3</sub>, CO and CH<sub>4</sub> also determine the  
77 concentration of OH (Leliveld et al., 2004). Prinn et al. (2005) suggested that major global  
78 wildfires and El Nino Southern Oscillation (ENSO) events could influence [OH] variability. A  
79 reduced number of small- to moderate-magnitude volcanic eruptions during the CH<sub>4</sub> stagnation  
80 period (Carn et al., 2015; Mills et al., 2015) may have increased [OH], due to increased  
81 downward UV radiation. Recently, Patra et al. (2014) analysed global CH<sub>3</sub>CCl<sub>3</sub> observations  
82 for 2004-2011 to derive the interhemispheric ratio of OH. In contrast to many model results  
83 which suggest higher mean [OH] in the north, they derived similar values for both hemispheres.

84 Warwick et al. (2002) investigated the impact of meteorology on atmospheric CH<sub>4</sub> growth rates  
85 from 1980 to 1998, i.e. well before the observed recent pause. They concluded that atmospheric  
86 conditions could be an important driver in the interannual variability (IAV) of atmospheric  
87 CH<sub>4</sub>. In similar studies a combination of atmospheric dynamics and changes in emissions were  
88 shown to explain some of the earlier past trends in atmospheric CH<sub>4</sub> (Fiore et al., 2006; Patra  
89 et al., 2009). This paper builds on these studies to investigate the chemical and non-chemical  
90 atmospheric contribution to the recent variations in CH<sub>4</sub> growth. By ‘non-chemical’ we mean  
91 transport-related influences, although the loss of CH<sub>4</sub> is ultimately due to chemistry as well.  
92 We use a global chemical transport model to simulate the period from 1993 to 2011 and to  
93 quantify the impact of variations in [OH] and meteorology on atmospheric CH<sub>4</sub> growth.

## 94 **2. Data and Models**

### 95 **2.1 NOAA and AGAGE CH<sub>4</sub> Data and Derived OH**

96 We have used surface CH<sub>4</sub> observations from 19 National Oceanographic and Atmospheric  
97 Administration/Earth System Research Laboratory (NOAA/ESRL) cooperative global air  
98 sampling sites (Dlugokencky et al., 2014) over 1993-2009 (see Table 1). To calculate the global  
99 average concentration, measurements were interpolated across 180 latitude bins, which were  
100 then weighted by surface area. We have also used the same method to derive global mean CH<sub>4</sub>  
101 based on 5 sites from the Advanced Global Atmospheric Gases Experiment (AGAGE) network  
102 (Prinn et al., 2000; Cunnold et al., 2002; Prinn et al., 2015).

103 Montzka et al. (2011) used measurements of methyl chloroform (CH<sub>3</sub>CCl<sub>3</sub>) from an  
104 independent set of flasks sampled at a subset of NOAA air sampling sites to derive global [OH]  
105 anomalies from 1997 to 2007. They argued that uncertainties in emissions are likely to limit  
106 the accuracy of the inferred inter-annual variability in global [OH], particularly before 1997.  
107 At this time the emissions were large but decreasing rapidly due to the phaseout of CH<sub>3</sub>CCl<sub>3</sub>  
108 production and consumption, and the large atmospheric gradients were also more difficult to  
109 capture accurately with only few measurement sites. Instrument issues caused an interruption  
110 to their CH<sub>3</sub>CCl<sub>3</sub> time series in 2008/9. We have averaged these (based on the red curve in  
111 Figure 3 of Montzka et al.) into yearly anomalies to produce relative interannual variations in  
112 the mean [OH]. Similarly, Rigby et al. (2013) used CH<sub>3</sub>CCl<sub>3</sub> measurements from the 5-station  
113 AGAGE network in a 12-box model to produce yearly global [OH] anomalies from 1995 (the  
114 date from which data from all 5 stations is available) to 2010. These two timeseries, which  
115 convert anomalies in the CH<sub>3</sub>CCl<sub>3</sub> decay rate into anomalies in [OH] using constant



116 temperature, correspond to the best estimate of [OH] variability from the two measurement  
117 networks by the groups who operate them. We then applied these two series of yearly anomalies  
118 uniformly to the global latitude-height [OH] field used in the recent TransCom CH<sub>4</sub> model  
119 intercomparison (see Patra et al., 2011), which itself was derived from a combination of semi-  
120 empirically calculated tropospheric OH distributions (Spivakovsky et al. 2000; Huijnen et al.,  
121 2010) and 2-D model simulated stratospheric loss rates (Velders, 1995). For consistency  
122 between the model experiments, both sets of yearly anomalies were scaled so that the mean  
123 [OH] between 1997 and 2007 (the overlap period where NOAA and AGAGE anomalies are  
124 both available) equalled the TransCom [OH] value. In the rest of this paper we refer to these  
125 two OH datasets as ‘NOAA-derived’ and ‘AGAGE-derived’.

126 These two calculations of yearly [OH] anomalies use slightly different assumptions for  
127 CH<sub>3</sub>CCl<sub>3</sub> emissions after 2002. Before that date they use values from Prinn et al. (2005). The  
128 NOAA data then assumed a 20% decay in emission for each subsequent year (Montzka et al.,  
129 2011), while AGAGE used United Nations Environment Programme (UNEP) consumption  
130 values (UNEP, 2015). Holmes et al. (2013) suggested that inconsistencies in CH<sub>3</sub>CCl<sub>3</sub>  
131 observations between the AGAGE and NOAA networks also limit understanding of OH  
132 anomalies for specific years due to an unexplained phasing difference of up to around 3 months.  
133 As we are interested in the impact of [OH] changes over longer time periods (e.g. 2000 – 2006),  
134 this phase difference will be less important. We have investigated the impact of the different  
135 CH<sub>3</sub>CCl<sub>3</sub> observations and assumed emissions on the derived [OH] anomalies (see Section  
136 3.1).

## 137 2.2 TOMCAT 3-D Chemical Transport Model

138 We have used the TOMCAT global atmospheric 3-D off-line CTM (Chipperfield, 2006) to  
139 model atmospheric CH<sub>4</sub> and CH<sub>3</sub>CCl<sub>3</sub> concentrations. The TOMCAT simulations were forced  
140 by winds and temperatures from the 6-hourly European Centre for Medium-Range Weather  
141 Forecasts (ECMWF) ERA-Interim reanalyses (Dee et al., 2011). They covered the period 1993  
142 to 2011 with a horizontal resolution of 2.8° × 2.8° and 60 levels from the surface to ~60 km.

143 The TOMCAT simulations use annually repeating CH<sub>4</sub> emissions, which have been scaled to  
144 previous estimates of 553 Tg/yr (Ciais et al., 2013), taken from various studies (Fiore et al.,  
145 2006; Curry et al., 2007; Bergamaschi et al., 2009; Pison et al., 2009; Spahni et al., 2011; Ito  
146 et al., 2012). Annually-repeating anthropogenic emissions (except biomass burning) were  
147 calculated from averaging the EDGAR v3.2 (2009) inventory from 1993 to 2009 (Olivier and  
148 Berowski, 2001). Biomass burning emissions were calculated using the GFED v3.1 inventory  
149 and averaged from 1997 to 2009 (van der Werf et al., 2010). The Joint UK Land Environment  
150 Simulator (JULES) (Best et al., 2011; Clark et al., 2011; Hayman et al., 2014) was used to  
151 calculate a wetland emission inventory between 1993 and 2009, which was then used to  
152 produce a scaled mean annual cycle. Annually-repeating rice (Yan et al., 2009), hydrate, mud  
153 volcano, termite, wild animal and ocean (Matthews et al., 1987) emissions were taken from the  
154 TransCom CH<sub>4</sub> study (Patra et al., 2011). The methane loss fields comprised an annually  
155 repeating soil sink (Patra et al., 2011), an annually repeating stratospheric loss field (Velders,



156 1995) and a specified [OH] field. The model was spun up for 15 years prior to initialising the  
157 simulations, using emission data from 1977 where available and annual averages otherwise.

158 Fifteen TOMCAT simulations were performed each with a CH<sub>4</sub> tracer and a CH<sub>3</sub>CCl<sub>3</sub> tracer.  
159 The runs had differing treatments of meteorology (winds and temperature) and [OH] (see Table  
160 2). Simulations with repeating [OH] fields (RE\_xxxx) used the TransCom dataset. The other  
161 runs with varying [OH] used the NOAA-derived or AGAGE-derived [OH] fields based on the  
162 original published work or our estimates (see Section 3.1). For these runs, the mean [OH] field  
163 is used where the respective NOAA or AGAGE-derived [OH] is unavailable or uncertain  
164 (before 1997 / after 2007 for NOAA and before 1997 / after 2009 for AGAGE). The five  
165 simulations with fixed wind and temperature fields (with labels ending in FTFW) used the  
166 ERA-Interim analyses from 1996 repeated for all years. The five simulations with varying  
167 winds and fixed temperature (with labels ending in FTVW) used zonal mean temperature fields  
168 averaged from 1993-2009. The OH anomalies are derived from the anomaly in the CH<sub>3</sub>CCl<sub>3</sub>  
169 loss rate, which combines variations in atmospheric OH concentration with variations in  
170 temperature which affect the rate constant of the CH<sub>3</sub>CCl<sub>3</sub> + OH reaction. To quantify the  
171 importance of this temperature effect we also performed 5 model runs which allow both winds  
172 and temperature to vary interannually according to ERA-Interim data (labels ending VTVW).

### 173 3. Results

#### 174 3.1 Correlation of CH<sub>4</sub> variations with OH and temperature

175 We first investigate the extent to which variations in the observed CH<sub>4</sub> growth rate correlate  
176 with variations in derived [OH]. Figure 1a shows the published NOAA-derived and AGAGE-  
177 derived global [OH] anomalies along with the annual CH<sub>4</sub> growth rate estimated from the  
178 NOAA and AGAGE measurements. The two [OH] series show the similar behaviour of  
179 negative anomalies around 1997 and 2006/7, and an extended period of more positive  
180 anomalies in between. For the time periods covered by the NOAA (1997-2007) and AGAGE  
181 (1997-2009) CH<sub>3</sub>CCl<sub>3</sub> observations, the two derived [OH] timeseries show negative correlations  
182 with the CH<sub>4</sub> growth from NOAA (regression coefficient, R = -0.32) and AGAGE (R = -0.64).  
183 Only the AGAGE [OH] correlation, from the longer timeseries, is statistically significant at the  
184 90% level.

185 We can use a simple ‘global box model’ (see Supplement S1) to estimate the [OH] variations  
186 required to fit the observed CH<sub>4</sub> growth rate variations assuming constant CH<sub>4</sub> emissions and  
187 temperature (black line in Figure 1b). This provides a crude guide to the magnitude of OH  
188 variations which could be important for changes in the CH<sub>4</sub> budget. Our results are consistent  
189 with those of Montzka et al. (2011) who performed a similar analysis on the NOAA CH<sub>4</sub> data.  
190 The required [OH] rarely exceeds their CH<sub>3</sub>CCl<sub>3</sub>-derived interannual variability (IAV) range  
191 of [OH] ( $\pm 2.3\%$ , shown as shading in the figure). Also shown in Figure 1b are the published  
192 estimates of the global mean OH anomalies from Figure 1a, converted to concentration units  
193 (see Section 2.1). The relative interannual variations in [OH] required to fit the CH<sub>4</sub>  
194 observations match the CH<sub>3</sub>CCl<sub>3</sub>-derived [OH] variations in many years, for example from  
195 1998-2002 (see Montzka et al., 2011). Some of the derived variations in [OH] exceed that



196 required to match the CH<sub>4</sub> growth rate, with larger negative anomalies in the early and later  
197 years and some slightly larger positive values in middle of the period.

198 Figures 1c and 1d show our estimates of [OH] using NOAA and AGAGE observations and  
199 two assumptions of post-2000 CH<sub>3</sub>CCl<sub>3</sub> emissions (see Section 2.1) in a global box model. The  
200 figures also compare our OH estimates with the NOAA-derived and AGAGE-derived [OH]  
201 anomalies based on the work of the observation groups (Figure 1a). Our results demonstrate  
202 the small impact of using different observations and post-2000 emission assumptions (compare  
203 filled and open red circles for the two panels). For these box model results there is also only a  
204 very small effect of using annually varying temperature (compare red and blue lines). In later  
205 years the choice of observations has a bigger impact than the choice of emissions on the derived  
206 [OH]. For AGAGE-derived values (Figure 1d) our estimates agree well with the published  
207 values of Rigby et al., (2013), despite the fact we use a global box model while they used a  
208 more sophisticated 12-box model. In contrast, there are larger differences between our values  
209 and the NOAA-derived OH variability published by Montzka et al. (2011) (Figure 1c), despite  
210 both studies using box models. In particular, around 2002-2003 we overestimate the positive  
211 anomaly in [OH]. We also estimate a much more negative OH anomaly in 1997 than Montzka  
212 et al., though we slightly underestimate the published AGAGE-derived anomaly in that year  
213 (Figure 1d). Tests show that differences between our results and the NOAA box model are due  
214 to the treatment of emissions. This suggests a larger uncertainty in the inferred low 1997 [OH]  
215 value, when emissions of CH<sub>3</sub>CCl<sub>3</sub> were decreasing rapidly, although reasons why atmospheric  
216 [OH] might have been anomalously low were discussed by Prinn et al. (2005). In the subsequent  
217 analysis we use the OH variability from the published NOAA and AGAGE studies as input to  
218 the 3-D model.

### 219 3.2 TOMCAT Simulations

220 Overall, Figure 1 shows the potential importance of small, observationally derived variations  
221 in OH concentrations to impact methane growth. We now investigate this quantitatively in the  
222 framework of a 3-D CTM.

#### 223 3.2.1 Methyl Chloroform

224 The TOMCAT simulations include a CH<sub>3</sub>CCl<sub>3</sub> tracer. This allows us to verify that our approach  
225 of using a global OH field, scaled by derived anomalies, allows the model to reproduce the  
226 observed magnitude and variability of CH<sub>3</sub>CCl<sub>3</sub> decay accurately. Figure 2a shows that the  
227 model, with the imposed [OH] field, does indeed simulate the global decay of CH<sub>3</sub>CCl<sub>3</sub> very  
228 well. This justifies our use of the ‘offline’ [OH] field, as models with interactive tropospheric  
229 chemistry can produce a large range in absolute global mean [OH] and therefore in lifetimes  
230 of gases such as CH<sub>3</sub>CCl<sub>3</sub>. For example, Voulgarakis et al., (2013) analysed the global mean  
231 [OH] from various 3D models and found a range of  $0.55 \times 10^6$  to  $1.34 \times 10^6$  molecules cm<sup>-3</sup>.  
232 Figure 2a also shows that the global mean CH<sub>3</sub>CCl<sub>3</sub> from the NOAA and AGAGE networks  
233 differ by ~2.5ppt around 1993-1996, but since then this difference has become smaller.

234 The observed and modelled CH<sub>3</sub>CCl<sub>3</sub> decay rate anomalies (calculated using the method of  
235 Holmes et al., (2013) with a 12-month smoothing) are shown in Figures 2b and 2c (different  
236 panels are used for AGAGE and NOAA comparisons for clarity). The model and observation-



237 derived results both tend to show a faster  $\text{CH}_3\text{CCl}_3$  decay (more positive anomaly) in the middle  
238 of the period, with slower decay at the start and end. The anomalies for the NOAA and  
239 AGAGE-derived OH show periodic variations on a timescale of 2-3 yrs but with a phase shift  
240 between the two datasets of 3 months, as noted by Holmes et al., (2013). The model runs with  
241 OH variability prescribed from the observations and varying winds also show these periodic  
242 variations with correlation coefficients ranging from 0.71 – 0.90. The correlation values for  
243 these runs using varying OH are all larger than the run using repeating OH (for RE\_FTVW  
244  $R=0.62$  compared to AGAGE data and 0.67 compared to NOAA data). Note that for  $\text{CH}_3\text{CCl}_3$   
245 decay there are only small differences between the 3-D simulations which use varying  
246 temperatures and the corresponding runs which use fixed temperature (e.g. simulation  
247 RE\_VTVW versus RE\_FTVW). This agrees with the results of Montzka et al (2011) based on  
248 their box model. This shows that the largest contribution from the  $\text{CH}_3\text{CCl}_3$  decay rate anomaly  
249 comes from variations in atmospheric OH concentration, rather than atmospheric temperature.  
250 The simulations with repeating winds show less variability in the  $\text{CH}_3\text{CCl}_3$  decay rate,  
251 particularly in the period 1999-2004, but the small difference suggests that the interannual  
252 variability in the observed  $\text{CH}_3\text{CCl}_3$  decay rate is driven primarily by the variations in the OH  
253 concentration. The remaining interannual variability in run RE\_FTVW is due to variations in  
254 emissions.

255 Figure 3 shows the  $\text{CH}_3\text{CCl}_3$  decay and decay rate anomalies at four selected stations, two from  
256 the NOAA network and two from the AGAGE network. The good agreement in the global  
257  $\text{CH}_3\text{CCl}_3$  decay in Figure 2 is also seen at these individual stations. At the AGAGE stations of  
258 Mace Head and Gape Grim, the model runs with varying OH perform better in capturing the  
259 decay rate anomalies than the runs with repeating OH. However, the impact of variability in  
260 the winds (solid lines versus dotted lines) is more apparent at these individual stations  
261 compared to the global means. At the NOAA station of Mauna Loa the model run with varying  
262 OH and varying winds also appears to perform better in capturing the observed variability in  
263  $\text{CH}_3\text{CCl}_3$  decay. At the South Pole the observed variability is small, except in 2000-2002. This  
264 feature is not captured by the model.

265 In summary, Figures 2 and 3 show that the global OH fields that we have constructed from  
266 different datasets can perform well in capturing the decay of  $\text{CH}_3\text{CCl}_3$  and its anomalies both  
267 globally and at individual stations. Although, the interannual variability in global mean OH has  
268 been derived from these  $\text{CH}_3\text{CCl}_3$  observations, the figures do show that the reconstructed  
269 model OH fields (which also depend on the methodology discussed in Section 2) perform well  
270 in simulating  $\text{CH}_3\text{CCl}_3$  within the 3D model. Therefore, we would argue that these fields are  
271 suitable for testing the impact of OH variability on the methane growth rate. Even so, it is  
272 important to bear in mind that these fields may not represent the true changes in atmospheric  
273 OH, particularly if the interannual variability in  $\text{CH}_3\text{CCl}_3$  emissions was a lot different to that  
274 assumed here. However, we would again note that we are focussing on the impact of multi-  
275 year variability which appears more robustly determined by the networks under differing  
276 assumptions of temperature and emissions than year-year variability.

277

### 278 3.2.2 Methane



279 Figure 4 shows deseasonalised modelled surface CH<sub>4</sub> from the 3-D CTM simulations compared  
280 with in-situ observations from a northern high-latitude station (Alert), two tropical stations  
281 (Mauna Loa and Tutuila), a southern high-latitude station (South Pole) and the global average  
282 of the NOAA and AGAGE stations. The global comparisons are shown for simulations both  
283 with varying and repeating meteorology. Figure 5 shows the global annual CH<sub>4</sub> growth rates  
284 with a 12-month smoothing (panel a) and differences between the model and NOAA and  
285 AGAGE observations (panels b and c). The changes in the modelled global mean CH<sub>4</sub> over  
286 different time periods are given in Table 3.

287 Figure 4 shows that in 1993, at the end of the model spin-up, the simulations capture the global  
288 mean CH<sub>4</sub> level well, along with the observed values at a range of latitudes. The exception is  
289 at high northern latitudes. However, these differences are not important when investigating the  
290 change in the global growth rate. The global change in atmospheric CH<sub>4</sub> in the simulations  
291 with varying winds for 1993 to the end of 2009 is between 75 and 104 ppb, compared to 56  
292 and 66 ppb in the observations.

293 Model run RE\_FTFW does not include interannual variations in atmospheric transport or CH<sub>4</sub>  
294 loss. Therefore, the modelled CH<sub>4</sub> gradually approaches a steady state value of ~1830 ppb  
295 (Figure 4f). The rate of CH<sub>4</sub> growth decreases from 7.9 ppb/yr (1993-1998) to 1.4 ppb/yr (2007-  
296 2009). Compared to run RE\_FTFW, the other simulations introduce variability on this CH<sub>4</sub>  
297 evolution.

298 Run RE\_FTVW includes interannual variability in wind fields which may alter the transport  
299 of CH<sub>4</sub> from the source (emission) to the sink regions. The largest difference between runs  
300 RE\_FTFW and RE\_FTVW occurs after 2000 (Figure 4f). During the stagnation period (1999-  
301 2006) run RE\_FTVW has a smaller growth rate of 3.5 ppb/yr compared to 4.1 ppb/yr in run  
302 RE\_FTFW, showing that variations in atmospheric transport made a small contribution to the  
303 slowdown in global mean CH<sub>4</sub> growth.

304 Compared to run RE\_FTVW, runs AP\_FTVW, AL\_FTVW, NP\_FTVW and NL\_FTVW  
305 include CH<sub>3</sub>CCl<sub>3</sub>-derived interannual variations in [OH] which introduce large changes in  
306 modelled CH<sub>4</sub>, which are more in line with the observations (Figure 4e and 5). These runs  
307 produce turnarounds in the CH<sub>4</sub> growth in 2001/2 (becomes negative) and 2005/6 (returns to  
308 being positive). For AGAGE-derived [OH] (runs AP\_FTVW, AL\_FTVW) the large negative  
309 anomaly in OH in 1997 produces a significant increase in CH<sub>4</sub> prior to the turnaround in 2001.

310 Table 3 summarises the change in global mean CH<sub>4</sub> over different time periods. These periods  
311 are defined by the key dates in the observed record, i.e. 1999 and 2006 as the start and end  
312 dates of the stagnation period. Comparison of Figure 4e and Table 3 shows, however, that the  
313 timing of the largest modelled change in growth rate do not necessarily coincide with those  
314 dates. That is understandable if other factors not considered here, e.g. emission changes, are  
315 contributing to the change in global CH<sub>4</sub> concentration. It does mean that the summary values  
316 in Table 3 do not capture the full impact of the changes in [OH] and winds within the stagnation  
317 period. Figure 4e shows that model runs with varying OH perform better in simulating the  
318 relative CH<sub>4</sub> trend 1999 to around 2004.



319 Table 3 shows that runs NP\_FTVW and NL\_FTVW (NOAA-derived [OH]) produce a small  
320 modelled CH<sub>4</sub> growth of 2.5-3.1 ppb/yr during the stagnation period 1999-2006, compared to  
321 1.0 ppb/yr for run AP\_FTVW (AGAGE-derived [OH]). The AGAGE results are slightly larger  
322 than the observed growth rate of 0.6-0.7 ppb/yr. Runs AL\_FTVW, AP\_FTVW, NL\_FTVW  
323 and NP\_FTVW capture the observed strong decrease in the CH<sub>4</sub> growth rate. Clearly, these  
324 runs demonstrate the significant potential for relatively small variations in mean [OH] to affect  
325 CH<sub>4</sub> growth. Excluding the stagnation period the mean modelled CH<sub>4</sub> lifetime in run  
326 NP\_FTVW is 9.4 years, but this decreases slightly by 0.01 years during the stagnation period.  
327 For run AP\_FTVW there is a decrease of 0.18 years from 9.6 years between the same intervals.  
328 The results from all the CTM simulations during 1999-2006 indicate that the accuracy of  
329 modelled CH<sub>4</sub> growth is improved by accounting for interannual variability in [OH] as derived  
330 from CH<sub>3</sub>CCl<sub>3</sub> observations, and interannual variability in meteorology.

331 The variation of [OH] after 2007 cannot be determined from the available NOAA data so run  
332 NP\_FTVW used the mean [OH] field for all subsequent years. The modelled CH<sub>4</sub> increase of  
333 3.5 ppb/yr underestimates the observations (4.9 ppb/yr). Should the lower [OH] of 2007 have  
334 persisted then the model would have produced a larger increase in CH<sub>4</sub>, in better agreement  
335 with the observations. The AGAGE-derived [OH] for 2007-2009 (run AP\_FTVW) produces a  
336 larger CH<sub>4</sub> growth relative to the previous years (8.8 ppb/yr). Runs RE\_FTFW (1.4 ppb/yr) and  
337 RE\_FTVW (1.8 ppb/yr) both show a decreased rate of growth during the final 5 years,  
338 consistent with a system approaching steady state.

339 Figure 5a shows the global CH<sub>4</sub> growth rate derived from the AGAGE and NOAA networks  
340 together with selected model simulations. Figures 5b and c show the differences between the  
341 model simulations and the NOAA and AGAGE observations, respectively. The runs which  
342 include variations in [OH] agree better with the observed changes, i.e. larger R values in panel  
343 (a) and the model lines are closer to the y=0 line in panels (b) and (c), especially in the first 5  
344 years of the stagnation period. It is interesting to note that the relative impacts of wind and  
345 temperature variations are larger for CH<sub>4</sub> than for CH<sub>3</sub>CCl<sub>3</sub> (compare simulations RE\_FTFW,  
346 RE\_FTVW and RE\_VTVW in Figures 2 and 5a). The temperature dependences of the OH loss  
347 reactions are similar for the two species (see Supplement S1) but the impact of transport from  
348 emissions regions to chemical loss regions is more variable for CH<sub>4</sub>. This needs to be considered  
349 when applying results derived from CH<sub>3</sub>CCl<sub>3</sub> to CH<sub>4</sub>.

#### 350 4. Discussion and Conclusions

351 Our model results suggest that variability in atmospheric [OH] and transport played key roles  
352 in the observed recent variations in CH<sub>4</sub> growth, particularly during the CH<sub>4</sub> stagnation period  
353 between 1999 and 2006. The 3-D CTM calculations show that during the stagnation period,  
354 variations in atmospheric conditions in the tropical lower to mid-troposphere could potentially  
355 account for an important component of the observed decrease in global CH<sub>4</sub> growth. Within  
356 this, small increases in [OH] were the largest factor, while variations in transport made a  
357 smaller contribution. Note again, however, that the ultimate loss of CH<sub>4</sub> is still due to  
358 chemistry. The role of atmospheric temperature variations is factored into the observationally  
359 derived OH, but model experiments show that changes in the OH concentration itself is most



360 important. The remainder of the variation can be ascribed to other processes not considered in  
361 our runs such as emission changes. There are also measurement uncertainties to consider and  
362 the possible underrepresentation of the global mean  $\text{CH}_3\text{CCl}_3$  which will affect the derived OH  
363 concentration. Our results are consistent with an earlier budget study which analysed 1991 to  
364 2004 and found that variations in [OH] were the main control of variations in atmospheric  $\text{CH}_4$   
365 lifetime (65%), with temperature accounting for a smaller fraction (35%) (Fiore et al., 2006).  
366 As we have noted here the  $\text{CH}_4$  lifetime can also be affected by emissions distributions which  
367 affects transport to the main loss regions.

368 Prior to the stagnation period the simulation using AGAGE-derived [OH] overestimates  $\text{CH}_4$   
369 growth when compared to observations which degrades the agreement with the observed  $\text{CH}_4$   
370 variations. A likely cause of this is inaccuracies in derived [OH] in 1997 when emissions still  
371 played a large role in the observed  $\text{CH}_3\text{CCl}_3$  and the e-fold decay had not yet stabilised  
372 (Montzka et al., 2011).

373 We have not accounted for expected variations in  $\text{CH}_4$  emissions in this study. We can conclude  
374 that although global  $\text{CH}_4$  emissions do vary year-to-year, the observed trend in  $\text{CH}_4$  growth  
375 between 1999 and 2006 was impacted by changing atmospheric processes that affected  $\text{CH}_4$   
376 loss. Changes in emissions are still important and likely still dominate  $\text{CH}_4$  variations over  
377 other time periods. The observed changes in growth rates during ENSO events in e.g. 1998 are  
378 poorly captured by the meteorological changes considered here and can be attributed to changes  
379 in emissions through changing precipitation and enhanced biomass burning (Hodson et al.,  
380 2011). The renewed growth of  $\text{CH}_4$  in 2007 is also poorly captured by all model simulations  
381 without varying [OH]. The observed decrease in AGAGE and NOAA-derived [OH] coincides  
382 with the increase in  $\text{CH}_4$  growth in 2007, although the currently available data do not allow for  
383 a more detailed investigation of the possible contribution of [OH] changes in this recent  
384 increase.

385 Despite the differences in year-to-year variability in [OH] derived from  $\text{CH}_3\text{CCl}_3$  observations  
386 (Holmes et al., 2013), we find that [OH] variability derived from two different networks of  
387 surface  $\text{CH}_3\text{CCl}_3$  observations over multi-year periods provide insights into atmospheric  $\text{CH}_4$   
388 variations. Improved quantification of the role of OH variability will require efforts to reduce  
389 uncertainties associated with estimating [OH]. Estimates of global mean [OH] in recent years  
390 from  $\text{CH}_3\text{CCl}_3$  observations is becoming increasingly difficult because  $\text{CH}_3\text{CCl}_3$  levels are  
391 currently  $<5$  ppt; hence this may limit the accuracy of derived [OH] and its variability in future  
392 years (Lelieveld et al., 2006). Wennberg et al. (2004) also noted that there can be time  
393 variations in the small uptake of  $\text{CH}_3\text{CCl}_3$  by the oceans, which can also affect the derived  
394 [OH] concentrations and are not considered here. Overall our study suggests that future  
395 atmospheric trends in  $\text{CH}_4$  are likely to be strongly influenced by not only emissions but also  
396 changes in processes that affect atmospheric loss. The accuracy of predictions would therefore  
397 be improved by including variations in [OH] and meteorology.

398 **Acknowledgements:** JRM thanks NERC National Centre for Earth Observation (NCEO) for  
399 a studentship. CW, MPC and MG acknowledge support from NERC grants GAUGE  
400 (NE/K002244/1) and AMAZONICA (NE/F005806/1). GDH acknowledges support from the



401 European Space Agency through its Support to Science Element initiative (ALANIS Methane),  
402 NCEO and the NERC MAMM grant (NE/I028327/1). SAM acknowledges support in part from  
403 NOAA Climate Program Office's AC4 program. AGAGE is supported by NASA grants  
404 NNX11AF17G to MIT and NNX11AF15G and NNX11AF16G to SIO, by NOAA, UK  
405 Department of Food and Rural Affairs (DEFRA) and UK Department for Energy and Climate  
406 Change (DECC) grants to Bristol University, and by CSIRO and Australian Bureau of  
407 Meteorology. MR is supported by a NERC Advanced Fellowship (NE/I021365/1). Model  
408 calculations were performed on the Arc1 and Archer supercomputers.

409 **References**

- 410 Bergamaschi, P., Frankenberg, C., Meirink, J. F., Krol, M., Villani, M. G., Houweling, S.,  
411 Dentener, F., Dlugokencky, E. J., Miller, J. B., Gatti, L. V., Engel, A., and Levin, I.:  
412 Inverse modeling of global and regional CH<sub>4</sub> emissions using SCIAMACHY satellite  
413 retrievals, *J. Geophys. Res.*, 114, 10.1029/2009jd012287, 2009.
- 414 Best, M. J., Pryor, M., Clark, D. B., Rooney, G. G., Essery, R. L. H., Ménard, C. B.,  
415 Edwards, J. M., Hendry, M. A., Porson, A., Gedney, N., Mercado, L. M., Sitch, S.,  
416 Blyth, E., Boucher, O., Cox, P. M., Grimmond, C. S. B., and Harding, R. J.: The Joint  
417 UK Land Environment Simulator (JULES), model description – Part 1: Energy and  
418 water fluxes, *Geosci. Model Dev.*, 4, 677–699, 10.5194/gmd-4-677-2011, 2011.
- 419 Bousquet, P., Ciais, P., Miller, J. B., Dlugokencky, E. J., Hauglustaine, D. A., Prigent, C.,  
420 Van der Werf, G. R., Peylin, P., Brunke, E. G., Carouge, C., Langenfelds, R. L.,  
421 Lathiere, J., Papa, F., Ramonet, M., Schmidt, M., Steele, L. P., Tyler, S. C., and White,  
422 J.: Contribution of anthropogenic and natural sources to atmospheric methane  
423 variability, *Nature*, 443, 439–443, 10.1038/nature05132, 2006.
- 424 Bousquet, P., Ringeval, B., Pison, I., Dlugokencky, E. J., Brunke, E. G., Carouge, C.,  
425 Chevallier, F., Fortems-Cheiney, A., Frankenberg, C., Hauglustaine, D. A., Krummel,  
426 P. B., Langenfelds, R. L., Ramonet, M., Schmidt, M., Steele, L. P., Szopa, S., Yver, C.,  
427 Viovy, N., and Ciais, P.: Source attribution of the changes in atmospheric methane for  
428 2006–2008, *Atmos. Chem. Phys.*, 11, 3689–3700, 10.5194/acp-11-3689-2011, 2011.
- 429 Carn, S. A., Yang, K., Prata, A. J., and Krotkov, N. A.: Extending the long-term record of  
430 volcanic SO<sub>2</sub> emissions with the Ozone Mapping and Profiler Suite nadir mapper,  
431 *Geophys. Res. Lett.*, 42, 925–932, 2015.
- 432 Chipperfield, M. P.: New version of the TOMCAT/SLIMCAT off-line chemical transport  
433 model: Intercomparison of stratospheric tracer experiments. *Q. J. R. Meteorol Soc.*,  
434 132, 1179–1203, 2006.
- 435 Ciais, P., Sabine, C., Bala, G., Bopp, L., Brovkin, V., Canadell, J., Chhabra, A., DeFries, R.,  
436 Galloway, J., Heimann, M., Jones, C., Le Quere, C., Myneni, R. B., Piao, S., and  
437 Thornton, P.: Carbon and other biogeochemical cycles, in: *Climate Change 2013: The*  
438 *Physical Science Basis. Contribution of Working Group I to the Fifth Assessment*  
439 *Report of the Intergovernmental Panel on Climate Change*, Cambridge University  
440 Press, 2013.
- 441 Cicerone, R. J., and Oremland, R. S.: Biogeochemical aspects of atmospheric methane,  
442 *Global Biogeochem. Cycles*, 2, 299–327, 1988.
- 443 Clark, D. B., Mercado, L. M., Sitch, S., Jones, C. D., Gedney, N., Best, M. J., Pryor, M.,  
444 Rooney, G. G., Essery, R. L. H., Blyth, E., Boucher, O., Harding, R. J., Huntingford,  
445 C., and Cox, P. M.: The Joint UK Land Environment Simulator (JULES), Model  
446 description – Part 2: Carbon fluxes and vegetation, *Geosci. Model Dev.*, 4, 701–722,  
447 10.5194/gmd-4-701-2011, 2011.
- 448 Cunnold, D., Steele, L., Fraser, P., Simmonds, P., Prinn, R., Weiss, R., Porter, L., O'Doherty,  
449 S., Langenfelds, R., and Krummel, P.: In situ measurements of atmospheric methane at



- 450 GAGE/AGAGE sites during 1985–2000 and resulting source inferences, *J. Geophys.*  
451 *Res.*, 107, ACH 20-21-ACH 20-18, 2002.
- 452 Curry, C. L.: Modeling the soil consumption of atmospheric methane at the global scale,  
453 *Global Biogeochem. Cycles*, 21, GB4012, doi:10.1029/2006GB002818, 2007.
- 454 Dee, D., Uppala, S., Simmons, A., Berrisford, P., Poli, P., Kobayashi, S., Andrae, U.,  
455 Balmaseda, M., Balsamo, G., Bauer, P., et al.: The ERA - Interim reanalysis:  
456 Configuration and performance of the data assimilation system, *Q. J. R. Meteorol. Soc.*,  
457 137, 553-597, 2011.
- 458 Dlugokencky, E. J., Houweling, S., Bruhwiler, L., Masarie, K., Lang, P., Miller, J., and Tans,  
459 P.: Atmospheric methane levels off: Temporary pause or a new steady - state?,  
460 *Geophys. Res. Lett.*, 30, doi:10.1029/2003GL018126, 2003.
- 461 Dlugokencky, E. J., Myers, R., Lang, P., Masarie, K., Crotwell, A., Thoning, K., Hall, B.,  
462 Elkins, J., and Steele, L.: Conversion of NOAA atmospheric dry air CH<sub>4</sub> mole fractions  
463 to a gravimetrically prepared standard scale, *J. Geophys. Res.*, 110, D18306, 2005.
- 464 Dlugokencky, E. J., Nisbet, E. G., Fisher, R., and Lowry, D.: Global atmospheric methane:  
465 budget, changes and dangers, *Philos. Trans. R. Soc. A*, 369, 2058-2072,  
466 10.1098/rsta.2010.0341, 2011.
- 467 Dlugokencky, E. J., P.M. Lang, A.M. Crotwell, K.A. Masarie, M.J. Crotwell, Atmospheric  
468 Methane Dry Air Mole Fractions from the NOAA ESRL Carbon Cycle Cooperative  
469 Global Air Sampling Network, 1983-2013, Version: 2014-06-24. Available at  
470 [ftp://aftp.cmdl.noaa.gov/data/trace\\_gases/ch4/flask/surface/](ftp://aftp.cmdl.noaa.gov/data/trace_gases/ch4/flask/surface/). Accessed July 6, 2014.
- 471 Etheridge, D. M., Steele, L. P., Francey, R. J., and Langenfelds, R. L.: Atmospheric methane  
472 between 1000 A.D. and present: Evidence of anthropogenic emissions and climatic  
473 variability, *J. Geophys. Res.*, 103, 15,979-15,993, 10.1029/98jd00923, 1998.
- 474 Fiore, A. M., Horowitz, L. W., Dlugokencky, E. J., and West, J. J.: Impact of meteorology  
475 and emissions on methane trends, 1990–2004, *Geophys. Res. Lett.*, 33, L12809,  
476 10.1029/2006gl026199, 2006.
- 477 Hayman, G.D., et al., Comparison of the HadGEM2 climate-chemistry model against in-situ  
478 and SCIAMACHY atmospheric methane data, *Atmos. Chem. Phys.*, 14, 13,257-13,280,  
479 2014.
- 480 Hodson, E. L., Poulter, B., Zimmermann, N. E., Prigent, C., and Kaplan, J. O.: The El Niño-  
481 Southern Oscillation and wetland methane interannual variability, *Geophys. Res. Lett.*,  
482 38, L08810, 10.1029/2011gl046861, 2011.
- 483 Holmes, C. D., Prather, M. J., Søvde, O., and Myhre, G.: Future methane, hydroxyl, and their  
484 uncertainties: key climate and emission parameters for future predictions, *Atmos.*  
485 *Chem. Phys.*, 13, 285-302, 2013.
- 486 Huijnen, V., Williams, J., Weele, M. v., Noije, T. v., Krol, M., Dentener, F., Segers, A.,  
487 Houweling, S., Peters, W., and de Laat, J.: The global chemistry transport model TM5:  
488 description and evaluation of the tropospheric chemistry version 3.0, *Geosci. Model*  
489 *Dev.*, 3, 445-473, 2010.



- 490 Ito, A., and Inatomi, M.: Use of a process-based model for assessing the methane budgets of  
491 global terrestrial ecosystems and evaluation of uncertainty, *Biogeosciences*, 9, 759-773,  
492 10.5194/bg-9-759-2012, 2012.
- 493 Kirschke, S., Bousquet, P., Ciais, P., Saunois, M., Canadell, J. G., Dlugokencky, E. J.,  
494 Bergamaschi, P., Bergmann, D., Blake, D. R., Bruhwiler, L., et al.: Three decades of  
495 global methane sources and sinks, *Nature Geosci.*, 6, 813-823, 2013.
- 496 Lelieveld, J., Dentener, F., Peters, W., and Krol, M.: On the role of hydroxyl radicals in the  
497 self-cleansing capacity of the troposphere, *Atmos. Chem. Phys.*, 4, 2337-2344, 2004.
- 498 Lelieveld, J., Brenninkmeijer, C. A. M., Joeckel, P., Isaksen, I. S. A., Krol, M. C., Mak, J. E.,  
499 Dlugokencky, E., Montzka, S. A., Novelli, P. C., Peters, W. and Tans, P. P.: New  
500 Directions: Watching over tropospheric hydroxyl (OH), *Atmospheric Environment*, 40,  
501 5741-5743, 2006.
- 502 Matthews, E., and Fung I.: Methane emissions from natural wetlands: Global distribution,  
503 area, and ecology of sources. *Global Biogeochem. Cycles*, 1, 61-86, 1987.
- 504 Mills, M. J., Schmidt, A., Easter, R., Solomon, S., Kinnison, D. E., Ghan, S. J., Neely III, R.  
505 R., Marsh, D. R., Conley, A., Bardeen, C. G., and Gettelman, A., Global volcanic  
506 aerosol properties derived from emissions, 1990-2014, using CESM1(WACCM), *J.*  
507 *Geophys. Res.* (under review), 2015.
- 508 Montzka, S. A., Krol, M., Dlugokencky, E., Hall, B., Jöckel, P., and Lelieveld, J.: Small  
509 interannual variability of global atmospheric hydroxyl, *Science*, 331, 67-69, 2011.
- 510 Myhre, G., Shindell, D., Bréon, F., Collins, W., Fuglestedt, J., Huang, J., Koch, D.,  
511 Lamarque, J., Lee, D., Mendoza, B., Nakajima, T., Robock, A., Stephens, G.,  
512 Takemura, T., and Zhang, H.: Anthropogenic and natural radiative forcing, in: *Climate*  
513 *Change 2013: The Physical Science Basis. Contribution of Working Group I to the*  
514 *Fifth Assessment Report of the Intergovernmental Panel on Climate Change*,  
515 Cambridge University Press, 2013.
- 516 Naik, V., Voulgarakis, A., Fiore, A. M., Horowitz, L., Lamarque, J.-F., Lin, M., Prather, M.  
517 J., Young, P., Bergmann, D., and Cameron-Smith, P.: Preindustrial to present-day  
518 changes in tropospheric hydroxyl radical and methane lifetime from the Atmospheric  
519 Chemistry and Climate Model Intercomparison Project (ACCMIP), *Atmos. Chem.*  
520 *Phys.*, 13, 5277-5298, 2013.
- 521 Nisbet, E. G., Dlugokencky, E. J., and Bousquet, P.: Atmospheric science. Methane on the  
522 rise - again, *Science*, 343, 493-495, 10.1126/science.1247828, 2014.
- 523 Olivier, J.G.J., Berdowski J.J.M.: Global emissions sources and sinks, in: *The Climate*  
524 *System*, edited by: Berdowski J, Guicherit R, and Heij BJ., IISBN 9058092550, A. A.  
525 Balkema Publishers/Swets & Zeitlinger Pub., Lisse, The Netherlands, 33-78, 2001.
- 526 Olivier, J. G., Van Aardenne, J. A., Dentener, F. J., Pagliari, V., Ganzeveld, L. N., and Peters,  
527 J. A.: Recent trends in global greenhouse gas emissions: regional trends 1970-2000 and  
528 spatial distribution of key sources in 2000, *Environmental Sciences*, 2, 81-99, 2005.
- 529 Patra, P. K., Takigawa, M., Ishijima, K., Choi, B.-C., Cunnold, D., J. Dlugokencky, E.,  
530 Fraser, P., J. Gomez-Pelaez, A., Goo, T.-Y., Kim, J.-S., Krummel, P., Langenfelds, R.,



- 531 Meinhardt, F., Mukai, H., O'Doherty, S., G. Prinn, R., Simmonds, P., Steele, P.,  
532 Tohjima, Y., Tsuboi, K., Uhse, K., Weiss, R., Worthly, D., and Nakazawa, T.: Growth  
533 rate, seasonal, synoptic, diurnal variations and budget of methane in the lower  
534 atmosphere, *J. Meteorol. Soc. Japan*, 87, 635-663, 10.2151/jmsj.87.635, 2009.
- 535 Patra, P. K., Houweling, S., Krol, M., Bousquet, P., Belikov, D., Bergmann, D., Bian, H.,  
536 Cameron-Smith, P., Chipperfield, M. P., and Corbin, K.: TransCom model simulations  
537 of CH<sub>4</sub> and related species: linking transport, surface flux and chemical loss with CH<sub>4</sub>  
538 variability in the troposphere and lower stratosphere, *Atmos. Chem. Phys.*, 11, 12,813-  
539 12,837, 2011.
- 540 Patra, P., Krol, M., Montzka, S., Arnold, T., Atlas, E., Lintner, B., Stephens, B., Xiang, B.,  
541 Elkins, J., and Fraser, P.: Observational evidence for interhemispheric hydroxyl-radical  
542 parity, *Nature*, 513, 219-223, 2014.
- 543 Pison, I., Bousquet, P., Chevallier, F., Szopa, S., and Hauglustaine, D.: Multi-species  
544 inversion of CH<sub>4</sub>, CO and H<sub>2</sub> emissions from surface measurements, *Atmos. Chem.*  
545 *Phys.*, 9, 5281-5297, 2009.
- 546 Pison, I., Ringeval, B., Bousquet, P., Prigent, C., and Papa, F.: Stable atmospheric methane in  
547 the 2000s: key-role of emissions from natural wetlands, *Atmos. Chem. Phys.*, 13,  
548 11,609-11,623, 10.5194/acp-13-11609-2013, 2013.
- 549 Prinn, R., Weiss, R., Fraser, P., Simmonds, P., Cunnold, D., Alyea, F., O'Doherty, S.,  
550 Salameh, P., Miller, B., and Huang, J.: A history of chemically and radiatively  
551 important gases in air deduced from ALE/GAGE/AGAGE, *J. Geophys. Res.*, 105,  
552 17,751-17,792, 2000.
- 553 Prinn, R. G.: Evidence for variability of atmospheric hydroxyl radicals over the past quarter  
554 century, *Geophys. Res. Lett.*, 32, L07809, 10.1029/2004gl022228, 2005.
- 555 Prinn, R.G., R.F. Weiss, P.J. Fraser, P.G. Simmonds, S. O'Doherty, P. Salameh, L. Porter, P.  
556 Krummel, R.H.J. Wang, B. Miller, C. Harth, B. Grealley, F.A. Van Woy, L.P. Steele, J.  
557 Mühle, G. Sturrock, F.N. Alyea, J. Huang, and D.E. Hartley, The ALE / GAGE  
558 AGAGE Network (DB1001), Carbon Dioxide Information Analysis Center (CDIAC),  
559 U.S. Department of Energy (DOE), <http://cdiac.esd.ornl.gov/ndps/alegagage.html>, 2015.
- 560 Rigby, M., Prinn, R. G., Fraser, P. J., Simmonds, P. G., Langenfelds, R., Huang, J., Cunnold,  
561 D. M., Steele, L. P., Krummel, P. B., and Weiss, R. F.: Renewed growth of atmospheric  
562 methane, *Geophys. Res. Lett.*, 35, L22805, 2008.
- 563 Rigby, M., Prinn, R. G., O'Doherty, S., Montzka, S. A., McCulloch, A., Harth, C. M., Mühle,  
564 J., Salameh, P., Weiss, R. F., and Young, D.: Re-evaluation of the lifetimes of the  
565 major CFCs and CH<sub>3</sub>CCl<sub>3</sub> using atmospheric trends, *Atmos. Chem. Phys.*, 13, 2691-  
566 2702, 2013.
- 567 Sander, S.P., et al., Chemical Kinetics and Photochemical Data for Use in Atmospheric  
568 Studies Evaluation Number 17. *JPL Publication 10-6*, Jet Propulsion Laboratory,  
569 Pasadena, USA, 2011.
- 570 Spahni, R., Wania, R., Neef, L., van Weele, M., Pison, I., Bousquet, P., Frankenberg, C.,  
571 Foster, P. N., Joos, F., Prentice, I. C., and van Velthoven, P.: Constraining global



- 572 methane emissions and uptake by ecosystems, *Biogeosciences*, 8, 1643-1665,  
573 10.5194/bg-8-1643-2011, 2011.
- 574 Spivakovsky, C., Logan, J., Montzka, S., Balkanski, Y., Foreman-Fowler, M., Jones, D.,  
575 Horowitz, L., Fusco, A., Brenninkmeijer, C., and Prather, M.: Three-dimensional  
576 climatological distribution of tropospheric OH: Update and evaluation, *J. Geophys.*  
577 *Res.*, 105, 8931-8980, 2000.
- 578 UNEP, The UNEP Environmental Data Explorer, as compiled from United Nations  
579 Environment Programme . United Nations Environment Programme.  
580 <http://ede.grid.unep.ch>, 2015.
- 581 van der Werf, G. R., Randerson, J. T., Giglio, L., Collatz, G., Mu, M., Kasibhatla, P. S.,  
582 Morton, D. C., DeFries, R., Jin, Y. v., and van Leeuwen, T. T.: Global fire emissions  
583 and the contribution of deforestation, savanna, forest, agricultural, and peat fires (1997–  
584 2009), *Atmos. Chem. Phys.*, 10, 11707-11735, 2010.
- 585 Velders, G. J. M.: Description of the RIVM 2-dimensional stratosphere model, RIVM  
586 Rapport 722201002, 1995.
- 587 Voulgarakis, A., Naik, V., Lamarque, J.-F., Shindell, D. T., Young, P., Prather, M. J., Wild,  
588 O., Field, R., Bergmann, D., and Cameron-Smith, P.: Analysis of present day and future  
589 OH and methane lifetime in the ACCMIP simulations, *Atmos. Chem. Phys.*, 13, 2563-  
590 2587, 2013.
- 591 Warwick, N. J., Bekki S., Law K. S., Nisbet E. G., and Pyle, J. A.: The impact of  
592 meteorology on the interannual growth rate of atmospheric methane, *Geophys Res Lett*,  
593 29, doi:10.1029/2002GL015282, 2002.
- 594 Wennberg, P. O., Peacock, S., Randerson, J. T., and Bleck, R.: Recent changes in the air -  
595 sea gas exchange of methyl chloroform, *Geophys. Res. Lett.*, 31, L16112, 2004.
- 596 Yan, X., Akiyama, H., Yagi, K., and Akimoto, H.: Global estimations of the inventory and  
597 mitigation potential of methane emissions from rice cultivation conducted using the  
598 2006 Intergovernmental Panel on Climate Change Guidelines, *Global Biogeochem.*  
599 *Cycles*, 23, GB2002, 10.1029/2008gb003299, 2009.
- 600



601 **Tables**

602

603 **Table 1.** List of NOAA and AGAGE stations which provided CH<sub>4</sub> and CH<sub>3</sub>CCl<sub>3</sub> observations.

Site Code	Site Name	Lat. (°N)	Lon. (°N)	Altitude (km)	CH <sub>4</sub>	CH <sub>3</sub> CCl <sub>3</sub>	Start Date <sup>++</sup>	End Date
ABP	Arembepe, Brazil	-12.77	-38.17	0	NOAA		27/10/2006	12/01/2010
ALT	Alert, Canada	82.45	-62.51	0.2	NOAA	NOAA	10/06/1985	Ongoing
ASC	Ascension Island, UK	7.97	-14.4	0.09	NOAA		11/05/1983	Ongoing
BRW	Barrow, USA	71.32	-156.61	0.01	NOAA	NOAA	06/04/1983	Ongoing
CGO	Cape Grim, Australia	-40.68	144.69	0.09	NOAA/AGAGE	NOAA/AGAGE	19/04/1984	Ongoing
HBA	Halley Station, UK	-75.61	-26.21	0.03	NOAA		17/01/1983	Ongoing
ICE	Storhofdi, Iceland	63.4	-20.29	0.12	NOAA		02/10/1992	Ongoing
KUM	Cape Kumukahi, USA	19.5	-154.8	0.02	-	NOAA	-	-
LEF	Park Falls, USA	45.9	-90.3	0.47	-	NOAA	-	-
MHD	Mace Head, Ireland	53.33	-9.9	0.01	NOAA/AGAGE	AGAGE**	03/06/1991	Ongoing
MLO	Mauna Loa, USA	19.54	-155.58	3.4	NOAA	NOAA	06/05/1983	Ongoing
NWR	Niwot Ridge, USA	40.05	-105.59	3.52	NOAA	NOAA	21/06/1983	Ongoing
PAL	Pallas-Sammaltunturi, Finland	67.97	24.12	0.56	NOAA		21/12/2001	Ongoing
PSA	Palmer Station, USA	-64.92	-64	0.01	NOAA	**	01/01/1983	Ongoing
RPB	Ragged Point, Barbados	13.17	-59.43	0.02	NOAA/AGAGE	AGAGE	14/11/1987	Ongoing
SEY	Mahe Island, Seychelles	-4.68	55.53	0	NOAA		12/05/1983	Ongoing
SMO	Tutuila, American Samoa	-14.25	-170.56	0.04	NOAA	NOAA/AGAGE	23/04/1983	Ongoing
SPO	South Pole, USA	-89.98	-24.8	2.81	NOAA	NOAA	20/02/1983	Ongoing
STM	Ocean Station M, Norway	66	2	0	NOAA		29/04/1983	27/11/2009
SUM	Summit, Greenland	72.6	-38.42	3.21	NOAA	**	23/06/1997	Ongoing
THD	Trinidad Head, USA	41.1	-124.1	0.1	AGAGE	AGAGE**	09/1995	Ongoing
ZEP	Ny-Alesund, Norway/Sweden	78.91	11.89	0.47	NOAA		11/02/1994	Ongoing

604

605 ++For NOAA CH<sub>3</sub>CCl<sub>3</sub> data the record starts in 1992 at 7 of the 9 stations used here. It started  
 606 in 1995 for KUM and 1996 for LEF.

607 \*\*NOAA flask data from these sites was not used in the present study or in Montzka et al.,

608 (2011).

609 **Table 2.** Summary of the fifteen TOMCAT 3-D CTM simulations.

Run	OH time variation	Meteorology <sup>b</sup>	
		Winds <sup>c</sup>	Temperature <sup>d</sup>
RE_FTFW	Repeating <sup>a</sup>	Fixed	Fixed
RE_FTVW	Repeating <sup>a</sup>	Varying	Fixed
RE_VTVW	Repeating <sup>a</sup>	Varying	Varying
AP_FTFW	AGAGE (Rigby et al., 2013)	Fixed	Fixed
AP_FTVW	AGAGE (Rigby et al., 2013)	Varying	Fixed
AP_VTVW	AGAGE (Rigby et al., 2013)	Varying	Varying
AL_FTVT	AGAGE (this work)	Fixed	Fixed
AL_FTVW	AGAGE (this work)	Varying	Fixed
AL_VTVW	AGAGE (this work)	Varying	Varying
NP_FTFW	NOAA (Montzka et al., 2011)	Fixed	Fixed
NP_FTVW	NOAA (Montzka et al., 2011)	Varying	Fixed
NP_VTVW	NOAA (Montzka et al., 2011)	Varying	Varying
NL_FTFW	NOAA (this work)	Fixed	Fixed
NL_FTVW	NOAA (this work)	Varying	Fixed
NL_VTVW	NOAA (this work)	Varying	Varying

610 a. Annually repeating [OH] taken from Patra et al. (2011).

611 b. Varying winds and temperatures are from ERA-Interim.

612 c. Fixed winds using repeating ERA-Interim winds from 1996.

613 d. Fixed temperatures use zonal mean ERA-Interim temperatures averaged over 1993-2009.



614 **Table 3.** Calculated methane changes over different time periods from selected TOMCAT  
 615 experiments and the NOAA and AGAGE observation networks.

Model run or observation network	Global mean $\Delta\text{CH}_4$ /ppb (ppb/yr)			
	2009-1993	1998-1993	2006-1999	2009-2007
RE_FTFW	85.0 (5.0)	47.2 (7.9)	32.9 (4.1)	4.3 (1.4)
RE_FTVW	82.2 (4.8)	48.2 (8.0)	27.8 (3.5)	5.4 (1.8)
RE_VTVW	74.6 (4.4)	45.6 (7.6)	23.1 (2.9)	5.3 (1.8)
AP_FTVW <sup>a</sup>	97.7 <sup>e</sup> (5.7)	62.3 <sup>e</sup> (10.4)	8.2 (1.0)	26.4 (8.8)
AL_FTVW <sup>b</sup>	104.2 <sup>e</sup> (6.1)	58.4 <sup>e</sup> (9.7)	17.3 (2.2)	27.5 (9.2)
NP_FTVW <sup>c</sup>	86.2 <sup>f</sup> (5.1)	49.7 <sup>f</sup> (8.3)	24.8 (3.1)	10.6 <sup>f</sup> (3.8)
NL_FTVW <sup>d</sup>	91.4 <sup>f</sup> (5.4)	58.8 <sup>f</sup> (9.8)	20.1 (2.5)	11.3 <sup>f</sup> (3.8)
NOAA obs.	56.1 (3.3)	36.0 (6.0)	4.8 (0.6)	14.7 (4.9)
AGAGE obs.	66.3 (3.9)	42.6 (7.1)	5.6 (0.7)	17.4 (5.8)

616

617 a. Taken from Rigby et al. (2013) and Patra et al. (2011).

618 b. Using 1997-2009 relative annual changes in mean [OH] derived from AGAGE data  
619 (Cunnold et al., 2002).

620 c. Taken from Montzka et al. (2011) and Patra et al. (2011).

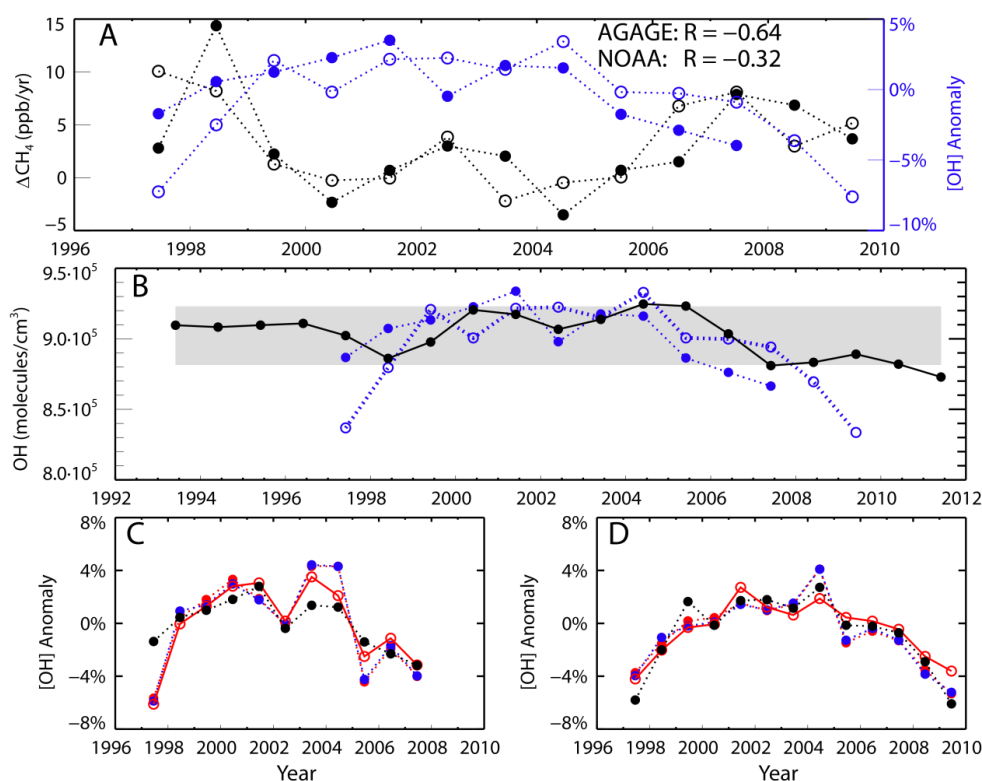
621 d. Using 1997-2007 relative annual changes in mean [OH] derived from NOAA data (Prinn  
622 et al., 2015).

623 e. Value using mean [OH] from 1993-1996.

624 f. Value using mean [OH] from 1993-1996 and 2008-2011.



625 **Figures**



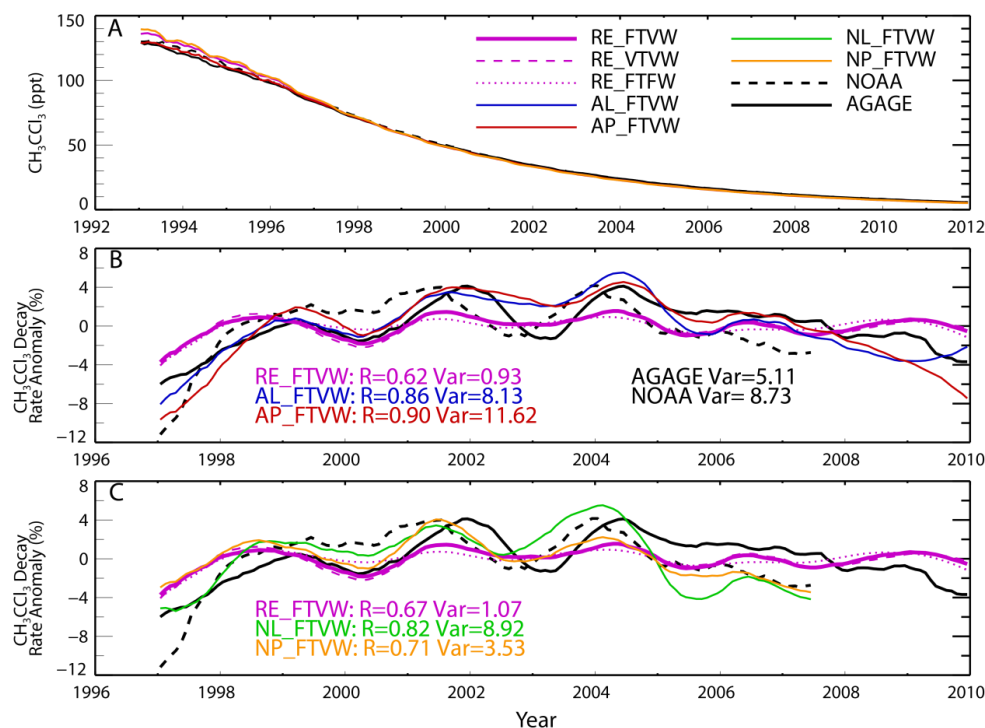
626

627 **Figure 1.** (a) Annual global CH<sub>4</sub> growth rate (ppb/yr) derived from NOAA (filled black circles)  
628 and AGAGE (open black circles) data (left hand y-axis), and published annual global [OH]  
629 anomalies derived from NOAA (filled blue circles, 1997-2007) and AGAGE (open blue  
630 circles, 1997-2009) CH<sub>3</sub>CCl<sub>3</sub> measurements (right hand y-axis) (see text). (b) Annual mean  
631 [OH] (molecules/cm<sup>3</sup>) required for global box model (see Supplement S1) to fit yearly  
632 variations in NOAA CH<sub>4</sub> observations assuming constant emissions and temperature ( $E=553$   
633 Tg/yr,  $T=272.9$  K), based on Montzka et al. (2011) (solid black line). The shaded region  
634 denotes [OH] deviation of  $\pm 2.3\%$  from the 1993-2011 mean. Also shown are the NOAA- and  
635 AGAGE-derived anomalies from panel (a) for an assumed mean OH (see Section 2.1). (c) Our  
636 estimates of [OH] derived from NOAA CH<sub>3</sub>CCl<sub>3</sub> calculated using a global box model  
637 (Supplement S1) using repeating (blue) and varying (red) annual mean temperature and the  
638 CH<sub>3</sub>CCl<sub>3</sub> emission scenario from UNEP (2015) (filled circles and dashed lines). Also shown  
639 for varying temperatures are results using the emissions of Montzka et al (2011) (red open  
640 circles and solid line) based on (Prinn et al. 2005) and the NOAA-derived values from panel  
641 (a) (black dashed line and circles). (d) As panel (c) but for OH derived from AGAGE CH<sub>3</sub>CCl<sub>3</sub>  
642 observations.

643

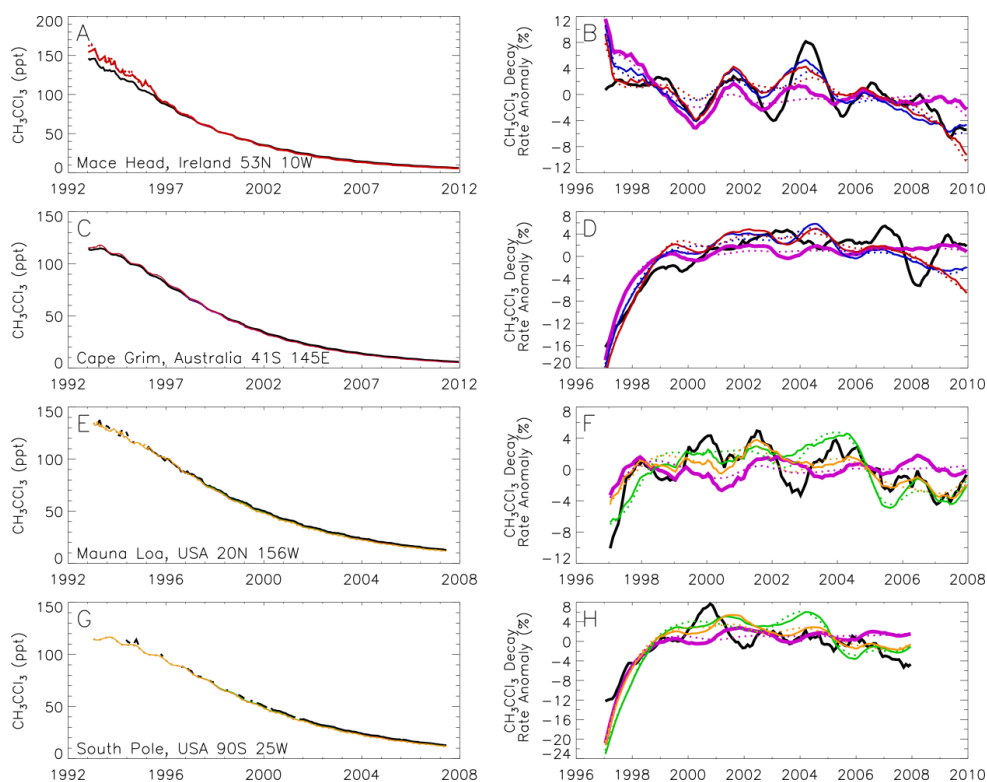


644



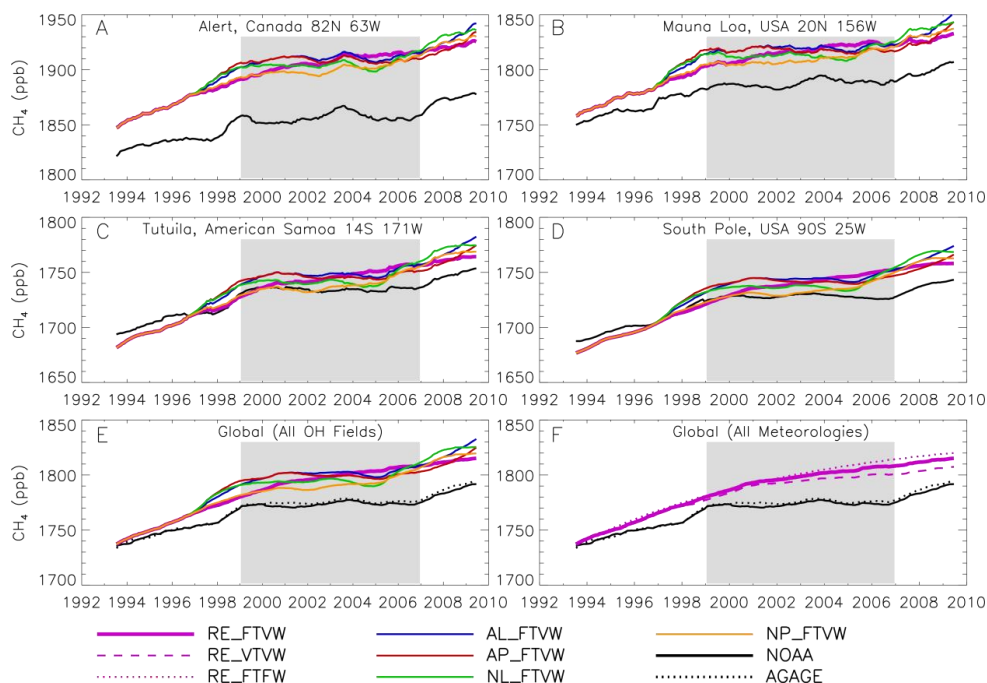
645

646 **Figure 2.** (a) Global mean surface  $\text{CH}_3\text{CCl}_3$  (ppt) from NOAA (black dashed) and AGAGE  
647 (black solid) observations from 1993 to 2012. Also shown are results from five TOMCAT  
648 simulations with fixed temperatures and varying winds (see Table 1). (b) Global surface  
649  $\text{CH}_3\text{CCl}_3$  decay rate anomalies from NOAA and AGAGE along with model runs RE\_FTVW,  
650 AL\_FTVW and AP\_FTVW (solid lines). Results from runs RE\_FTVW and RE\_VTVW are  
651 shown as a purple dotted line and dashed line, respectively. Observation and model anomalies  
652 are smoothed with a 12-month running average. Values given represent correlation coefficient  
653 when compared to AGAGE observations and variance. The decay rate anomaly is calculated  
654 from global mean  $\text{CH}_3\text{CCl}_3$  values using equation (1) from Holmes et al., (2013), expressed as  
655 a percentage of the typical decay with a 12-month smoothing. (c) As panel (b) but for model  
656 runs NL\_FTVW and NP\_FTVW, along with RE\_FTVW, RE\_VTVW and RE\_FTFW, and  
657 correlation coefficients for comparison with NOAA observations. The model results are split  
658 across panels (b) and (c) for clarity.

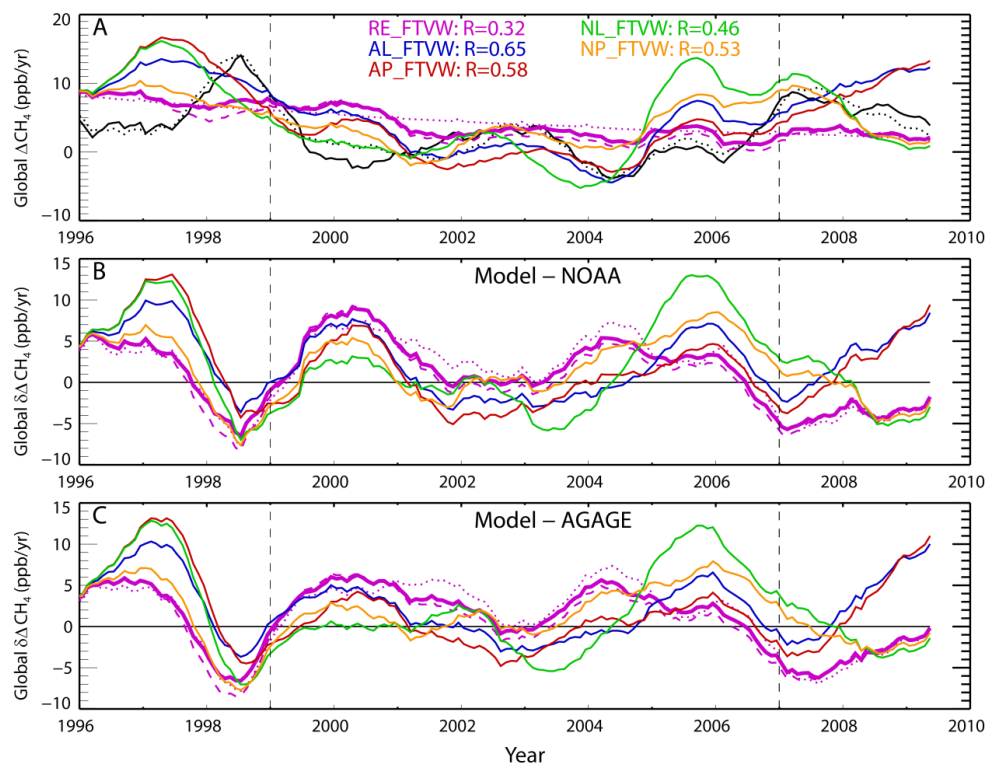


659

660 **Figure 3.** (Left) Observed mean surface  $\text{CH}_3\text{CCl}_3$  (ppt) (black line) from (a) Mace Head  
661 (AGAGE), (c) Cape Grim (AGAGE), (e) Mauna Loa (NOAA) and (g) South Pole (NOAA).  
662 Also shown are results from five TOMCAT simulations with fixed temperatures and varying  
663 winds (FTVW, for legend see Figure 2a). (Right): Surface  $\text{CH}_3\text{CCl}_3$  decay rate anomalies at the  
664 same station as the corresponding left column plot for observations (black), TOMCAT  
665 simulations with varying winds (FTVW, solid coloured lines) and TOMCAT simulations with  
666 fixed winds (FTFW, dotted lines). Comparisons at NOAA (AGAGE) stations show only  
667 comparisons with runs using NOAA (AGAGE)-derived OH, along with runs RE\_FTVW and  
668 RE\_FTFW in all panels.



670 **Figure 4.** (a, b, c and d) Deseasonalised surface CH<sub>4</sub> (ppb) from 4 NOAA sites (black solid line)  
 671 from 1993 to 2009. Also shown are results from five TOMCAT 3-D CTM simulations with  
 672 fixed temperatures and varying winds (FTVW, see **Table 2**). (e) Deseasonalised global mean  
 673 surface CH<sub>4</sub> from NOAA (black solid) and AGAGE (black dashed) observations along with  
 674 five TOMCAT simulations with different treatments of OH. (f) Same as (e) but for TOMCAT  
 675 simulations using repeating OH (RE) and different treatments of winds and temperature. All  
 676 panels use observation and model values which are smoothed with a 12-month running  
 677 average. The shaded region marks the stagnation period in the observed CH<sub>4</sub> growth rate.



678

679 **Figure 5.** (a) The smoothed variation in the global annual CH<sub>4</sub> growth rate (ppb/yr) derived from NOAA (black solid) and AGAGE (black dashed) observations. Also shown are the smoothed growth rates from five TOMCAT 3-D CTM simulations with fixed temperatures and varying winds (FTVW, see Table 1). Values in legend give correlation coefficient between model run and NOAA observations. Also shown are results from runs RE\_FTVW and RE\_VTVW as a purple dotted line and dashed line, respectively (b) The difference in smoothed growth rate between TOMCAT simulations and NOAA observations shown in panel (a). (c) Same as (b) except using differences compared to AGAGE observations. The vertical dashed lines mark the start and end of the stagnation period in the observed CH<sub>4</sub> growth rate (1999 – 688 2006).